AGN Physics with the Sloan Digital Sky Survey
*ASP Conference Series, Vol. **VOLUME***, 2004*
G.T. Richards and P.B. Hall, eds.

Relativistic Outflows in AGNs

Nektarios Vlahakis[†] & Arieh Königl

Department of Astronomy & Astrophysics, University of Chicago, 5640 S. Ellis Ave., Chicago, IL 60637, USA

Abstract. There are observational indications that relativistic outflows in AGNs are accelerated over distances that far exceed the scale of the central engine. Examples include the radio galaxy NGC 6251, where knots in the radio jets were inferred to accelerate from ~ 0.13 c at a distance of ~ 0.53 pc from the galactic nucleus to ~ 0.42 c at $r = 1.0$ pc, and the quasar 3C 345, where the Lorentz factor of the radio knot C7 was deduced to increase from ~ 5 to > 10 as it moved from $r = 3$ pc to $r = 20$ pc. It is argued, using exact semianalytic solutions of the relativistic MHD equations, that this behavior is a signature of magnetic acceleration. The same basic driving mechanism may apply to the relativistic jets in AGNs, gamma-ray burst sources, and microquasars.

1. Introduction

Magnetic acceleration has long been considered an attractive mechanism for the origin of AGN jets (e.g., Blandford & Payne 1982). These models have commonly been thought to imply that the bulk of the acceleration occurs fairly close to the source, as in thermally driven outflows. Since the region near the central black hole cannot be resolved, it has been unclear whether one could observationally infer that magnetic driving actually takes place. Recent theoretical work has, however, established that magnetic acceleration can occur over many decades in radius, for both nonrelativistic (Vlahakis et al. 2000) and relativistic (Li et al. 1992; Vlahakis & Königl 2003a, hereafter VK) outflows. There are already a number of AGNs for which there is direct observational evidence for acceleration to relativistic speeds occurring in an extended (parsec-scale) region. The acceleration on scales that are much larger than the gravitational radius of the central object cannot be easily explained in terms of thermal driving (Vlahakis & Königl 2003b). Thus, magnetic driving is the most plausible interpretation of the observed parsec-scale accelerations. Here we discuss two examples (a radio galaxy and a blazar) and argue that they provide strong support for magnetic stresses as the dominant acceleration mechanism.

[†]Present address: Section of Astrophysics, Astronomy & Mechanics, Department of Physics, University of Athens, 15784 Zografos Athens, Greece

2. The Relativistic MHD Model and Applications to AGN Outflows

The system of equations of special-relativistic, ideal MHD consists of the Maxwell and Euler equations together with the mass and specific-entropy conservation relations. Assuming axisymmetry [$\partial/\partial\phi = 0$ in spherical $(r\,,\theta\,,\phi)$ and cylindrical $(\varpi\,,\phi\,,z)$ coordinates] and a steady state, the full set of equations can be partially integrated to yield several field-line constants. These constants are the total specific angular momentum $L(A)$, the field angular velocity $\Omega(A)$, the "magnetization parameter" $\sigma_{\rm M}(A)$ (with the mass-to-magnetic flux ratio given by $A\Omega^2/\sigma_{\rm M}c^3$), the adiabat $Q(A) \equiv P/\rho_0^{5/3}$, and the total energy-to-mass flux ratio $\mu(A)c^2 = \xi\gamma c^2 + (c/4\pi)(E|B_\phi|/\gamma\rho_0 V_p)$. Here A is the poloidal magnetic flux function (which identifies the field line), $\xi c^2 = c^2 + 5P/2\rho_0$ is the specific enthalpy, $\mathbf{V}$ is the bulk velocity, γ is the Lorentz factor, ρ_0 and P are the comoving matter density and pressure, $\mathbf{E}$ and $\mathbf{B}$ are the electric and magnetic fields, and the subscripts p and ϕ denote poloidal and azimuthal vector components, respectively. VK integrated the two remaining relations (the Bernoulli and transfield force-balance equations) assuming radial self-similarity of the form $r = \mathcal{F}_1(A)\mathcal{F}_2(\theta)$. With this ansatz it is possible to separate the $(A\,,\theta)$ variables if the following relations hold: $\mathcal{F}_1(A) \propto A^{1/F}$, $L(A) \propto A^{1/F}$, $\Omega(A) \propto A^{-1/F}$, $Q(A) \propto A^{-2(F-2)/3}$, $\mu(A) = const$, and $\sigma_{\rm M}(A) = const$ (see Li et al. 1992 and Contopoulos 1994 for the "cold" limit of this model). The parameter F controls the current distribution: $\varpi|B_\phi| = A^{1-1/F}\mathcal{F}(\theta)$. Close to the origin the field is force-free: $\mathcal{F}(\theta) \approx const$, and hence $\varpi|B_\phi| \propto A^{1-1/F}$. Thus, the parameter regime $F > 1$ corresponds to a current-carrying jet, which is applicable near the rotation axis, whereas $F < 1$ corresponds to the return-current regime, which possibly occurs at large cylindrical distances. The remaining task is to integrate ordinary differential equations and find solutions crossing the Alfvén and modified-fast magnetosonic singular points. We now apply this formalism to the interpretation of accelerating relativistic jets in two AGNs, the powerful radio galaxy NGC 6251 and the quasar 3C 345.

VLBI measurements indicate sub–parsec-scale acceleration of the radio jet and counterjet in NGC 6251 from $V(r = 0.53\ {\rm pc}) = 0.13c$ to $V(r = 1\ {\rm pc}) = 0.42c$ (Sudou et al. 2000). Magnetic acceleration can naturally account for these observations, as demonstrated with a specific solution in Figure 1. Panels (c)–(g) in this figure show various quantities as functions of $\varpi/\varpi_{\rm A}$ (which, in turn, is a function of the polar angle θ) along the outermost field line. (Here $\varpi_{\rm A}$ is the Alfvén lever arm, and $\varpi_{\rm A,out} = 10^3\,\varpi_{\rm A,in} = 0.98$ pc in this example.) Panel (c) depicts the force densities in the poloidal direction, showing that thermal and centrifugal effects are important only near the origin, with the magnetic pressure-gradient force rapidly becoming the dominant driving mechanism. The same conclusion can be drawn from the plot of the energy flux components in panel (d): acceleration driven by the conversion of enthalpy into kinetic energy occurs only near the origin, where $\xi\gamma > \gamma$. In this region the field is nearly force-free and the Poynting-to-mass flux ratio remains roughly constant. Beyond the point where $\xi\gamma \approx \gamma$ the magnetic acceleration takes over: in this regime the increase in the Lorentz factor results from a decrease in the Poynting-to-mass flux ratio. Asymptotically, an approximate equipartition between the kinetic and Poynting fluxes is attained. Panels (e) and (f) depict the bulk velocity

components and the temperature, respectively. Even if the initial temperature is as high as $\sim 10^{12}$ K, thermal effects are overall insignificant. Panel (g) shows that the magnetic field is primarily poloidal near the origin of the flow but becomes predominantly azimuthal further downstream. Asymptotically, $B_z \propto \varpi^{-2}$, $-B_\phi \propto \varpi^{-1}$; also $B_\varpi << B_z$ — a signature of cylindrical collimation.

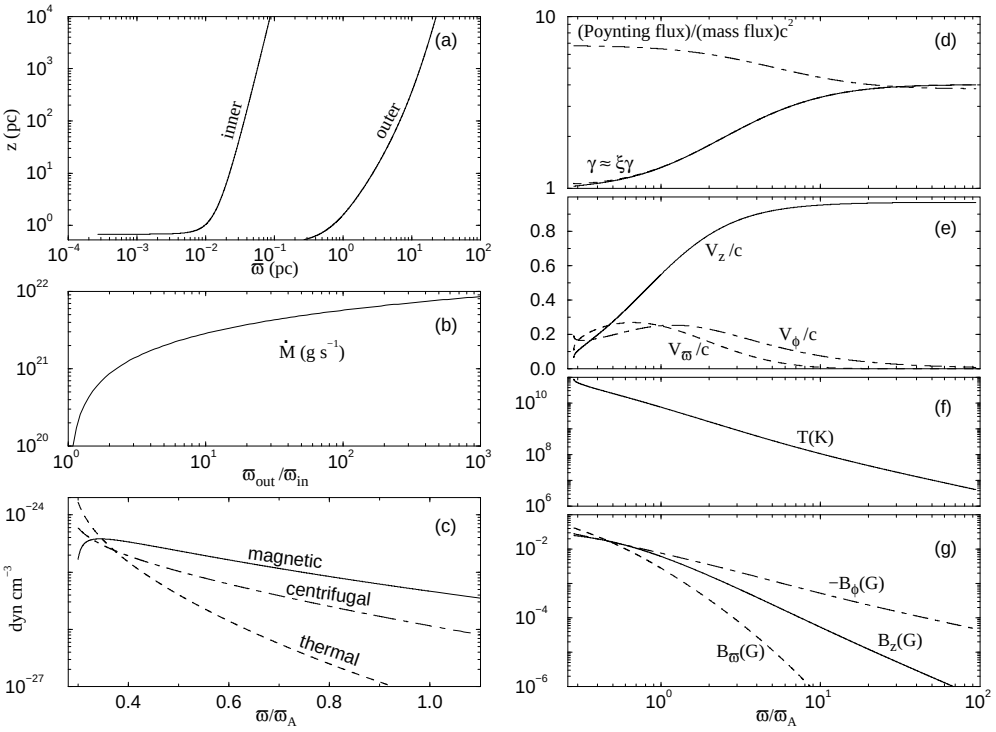

Figure 1. r self-similar solution describing the jets in NGC 6251. (a) Poloidal field-line shape on a logarithmic scale. (b) Mass-loss rate as a function of $\varpi_{\rm out}/\varpi_{\rm in}$, the ratio of the outermost and innermost disk radii. The remaining panels are discussed in the text.

VLBI images of the quasar 3C 345 indicate that the jet components' speeds increase with separation from the core (Zensus, Cohen, & Unwin 1995; Lobanov & Zensus 1999). In particular, in the case of the C7 component, Unwin et al. (1997) inferred that it accelerates from $\gamma \sim 5$ to $\gamma \gtrsim 10$ over the (deprojected) distance range (measured from the core) $\sim 3 - 20$ pc. We propose that this pc-scale acceleration is again most plausibly interpreted in terms of magnetic driving, and we present in Figure 2 a particular solution for a magnetically driven proton-electron jet that supports this conclusion. For the adopted fiducial parameters, the C7 component is expected to continue to accelerate up to $\gamma_\infty \approx 30$: values of this order may, in fact, characterize the more distant components (in particular, C3 and C5) of the 3C 345 jet (Lobanov & Zensus 1999). The pc-scale helical field morphology implied by our model is consistent with VLBI polarization maps of BL Lac objects (e.g., Gabuzda, Pushkarev, & Cawthorne 2000) and circular polarization measurements of blazars (e.g., Homan, Attridge, & War-

dle 2001). As discussed in VK, the same basic model may also account for the collimated relativistic outflows in gamma-ray burst sources and microquasars.

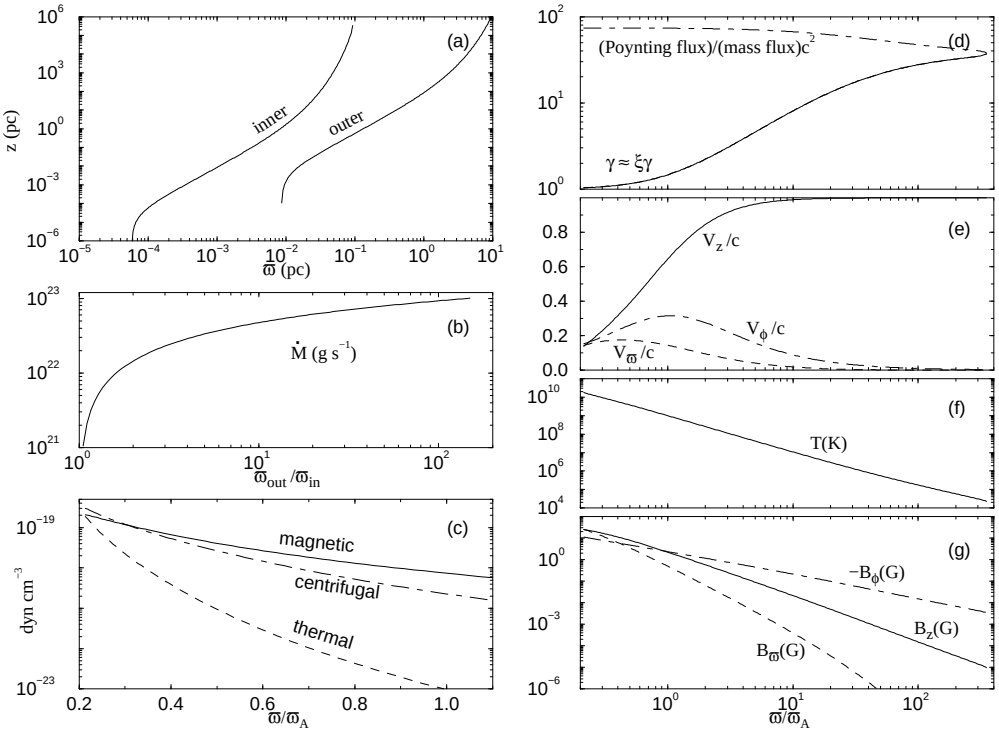

Figure 2. Same as Fig. 1, but for the application to the superluminal jet in 3C 345. Here $\varpi_{\rm A,out} = 150\,\varpi_{\rm A,in} = 4.1 \times 10^{-2}$ pc.

References

Blandford, R. D., & Payne, D. G. 1982, MNRAS, 199, 883

Contopoulos, J. 1994, ApJ, 432, 508

Gabuzda, D. C., Pushkarev, A. B., & Cawthorne, T. V. 2000, MNRAS, 319, 1109

Homan, D. C., Attridge, J. M., & Wardle, J. F. C. 2001, ApJ, 556, 113

Li, Z.-Y., Chiueh, T., & Begelman, M.C. 1992, ApJ, 394, 459

Lobanov, A. P. & Zensus J. A. 1999, ApJ, 521, 509

Sudou, H., et al. 2000, PASJ, 52, 989

Unwin, S. C., et al. 1997, ApJ, 480, 596

Vlahakis, N. & Königl, A. 2003a, ApJ, 596, 1080 (VK)

Vlahakis, N. & Königl, A. 2003b, ApJ, submitted

Vlahakis, N., Tsinganos, K., Sauty, C., & Trussoni, E. 2000, MNRAS, 318, 417

Zensus J. A., Cohen, M. H., & Unwin, S. C. 1995, ApJ, 443, 35